Status Report, April 1, 1991:
Viscoelastic Deformation Near Active Plate Boundaries
NAG 5-750

Steven N. Ward
Institute of Tectonics
University of California, Santa Cruz

Sections **A-B** below document some of our recent progress under this project and offer several potential routes for the future.

A. Kinematics of Global Plate Motions and Regional Deformation from VLBI.

Very Long Baseline Interferometry now has the capacity to monitor geodetic positions with precisions of a few 1 mm over continental baselines. For tectonic applications, one of the major products of the VLBI program is the determination of the rate of change of station locations. Vector site velocities are now routinely produced by many groups, including ours. We believe that the emphasis in the future will be less on the production vector site velocities and more on their interpretation. We are well positioned in this arena, having been in the forefront in drawing inferences from VLBI data concerning plate tectonics, plate stability, regional deformation and fault slip rates. Below we touch upon one of the novel techniques developed by our group in the past two years, VLBI Euler poles.

A.1. Theory: Euler Poles from VLBI

Euler poles provide a means to simplify the kinematics of a possibly complicated vector field on the surface of a sphere. In the late 1960's, application of Euler poles to lithospheric motions provided a major impetus for plate tectonic theory to sweep the scientific community. The use of Euler poles in interpreting space geodetic data has found similar success.

A typical space geodetic data set produced by NASA (Figure 1) consists of $N(\approx 300)$ length (B_{ij}) and transverse (T_{ij}) velocities determined among $M(\approx 30)$ stations. Reduction of the baseline data to a set of vector site velocities is straightforward [*Ward*, 1988]. Local north $[v_i^n \hat{\mathbf{n}}_i,\ v_j^n \hat{\mathbf{n}}_j]$ and local east $[v_i^e \hat{\mathbf{e}}_i,\ v_j^e \hat{\mathbf{e}}_j]$ velocities of sites at $\mathbf{P}_i$ and $\mathbf{P}_j$ are linked to the observed baseline B_{ij} and transverse T_{ij} rates by

$$\underset{(N\times 1)}{\begin{bmatrix} B_{ij} \\ T_{ij} \\ \vdots \end{bmatrix}} = \underset{(N\times 2M)}{\begin{bmatrix} \hat{\mathbf{b}}_{ij}\cdot\hat{\mathbf{n}}_i & \hat{\mathbf{b}}_{ij}\cdot\hat{\mathbf{e}}_i & -\hat{\mathbf{b}}_{ij}\cdot\hat{\mathbf{n}}_j & -\hat{\mathbf{b}}_{ij}\cdot\hat{\mathbf{e}}_j \\ \hat{\mathbf{t}}_{ij}\cdot\hat{\mathbf{n}}_i & \hat{\mathbf{t}}_{ij}\cdot\hat{\mathbf{e}}_i & -\hat{\mathbf{t}}_{ij}\cdot\hat{\mathbf{n}}_j & -\hat{\mathbf{t}}_{ij}\cdot\hat{\mathbf{e}}_j \\ \vdots & \vdots & \vdots & \vdots \end{bmatrix}} \underset{(2M\times 1)}{\begin{bmatrix} v_i^n \\ v_i^e \\ v_j^n \\ v_j^e \\ \vdots \end{bmatrix}} \qquad (1)$$

where

$$\hat{\mathbf{b}}_{ij} = (\mathbf{P}_i - \mathbf{P}_j)/\,|\,\mathbf{P}_i - \mathbf{P}_j\,|$$

and

$$\hat{\mathbf{t}}_{ij} = \mathbf{P}_i \times \mathbf{P}_j/\,|\,\mathbf{P}_i \times \mathbf{P}_j\,|$$

After being weighted by their respective uncertainties, the N equations (1) are inverted to obtain $2M$ velocity components v_i^n, v_i^e and their uncertainties $\mathbf{cov}[v_i^n v_i^e]$. Rigid plate tectonic

models are devised by fitting Q groups of vector site velocities with equations of the form

$$\mathbf{V}_v(\mathbf{P}_i^q) = \underset{(2m_q \times 1)}{\begin{bmatrix} v_i^n \\ v_i^e \\ \vdots \end{bmatrix}} = \underset{(2m_q \times 1)}{\begin{bmatrix} \hat{\mathbf{n}}_i^q \cdot [\boldsymbol{\Omega}_q \times \mathbf{P}_i^q] \\ \hat{\mathbf{e}}_i^q \cdot [\boldsymbol{\Omega}_q \times \mathbf{P}_i^q] \\ \vdots \end{bmatrix}} =$$

$$\underset{(2m_q \times 3)}{\begin{bmatrix} (\mathbf{P}_i^q \times \hat{\mathbf{n}}_i^q)_x & (\mathbf{P}_i^q \times \hat{\mathbf{n}}_i^q)_y & (\mathbf{P}_i^q \times \hat{\mathbf{n}}_i^q)_z \\ (\mathbf{P}_i^q \times \hat{\mathbf{e}}_i^q)_x & (\mathbf{P}_i^q \times \hat{\mathbf{e}}_i^q)_y & (\mathbf{P}_i^q \times \hat{\mathbf{e}}_i^q)_z \\ \vdots & \vdots & \vdots \end{bmatrix}} \underset{(3 \times 1)}{\begin{bmatrix} (\Omega_q)_x \\ (\Omega_q)_y \\ (\Omega_q)_z \end{bmatrix}} \qquad (2)$$

The $\boldsymbol{\Omega}_q$ $(q = 1, Q)$ are Euler poles, constant over the m_q VLBI sites assigned to the q-th plate.

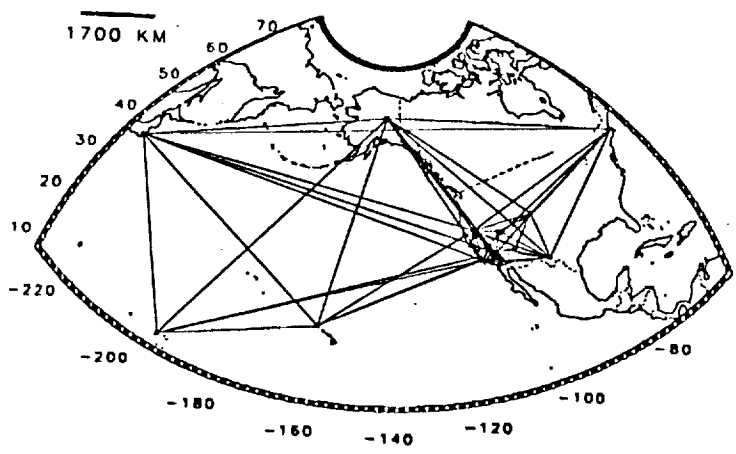

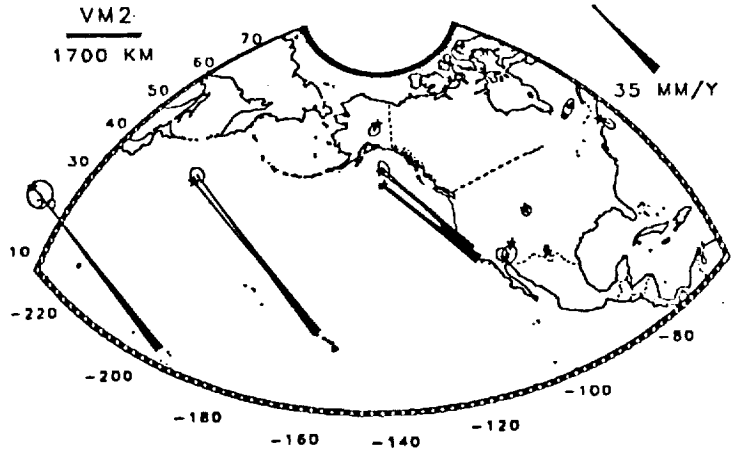

Fig. 1. Left. Map illustrating 113 VLBI baselines in North America and the Pacific Rim. The dense network in the far western United States provides a detailed picture of plate boundary deformation. Sites elsewhere in stable North America and the mid-Pacific provide estimates of relative plate motion unbiased by plate boundary deformation.

Fig. 2. Right. Plots of observed $\mathbf{V}_o(\mathbf{P}_i)$ (solid arrows) and theoretical $\mathbf{V}_p(\mathbf{P}_i)$ (starred vectors) site velocities for VM2 at the ten interior sites. VM2 corrects the systematic misfit of NUVEL and fits the velocities of the ten stable sites within 2.5 σ. The remaining error reflects the degree of consistency of VLBI data and the rigid plate assumption at the ten sites. The triangle, circle, and inverted triangle in eastern Canada are the RM2, NUVEL, and VM2 Pacific-North America poles. All errors are 3σ.

Construction of plate models is an important advancement beyond free-site inversions (1). By determining the Euler poles of a few plates upon which several stations ride, bias and errors in the velocities of individual sites can be averaged out and failures of the rigid plate assumption will be easy to document. In addition, this approach makes it possible to quantify the consistency of specified plate models against the VLBI data set as a whole, and not just individual baseline rates or site vectors.

A.2. Global Plate Models.

One of the original tasks envisioned for space geodesy was the confirmation or confrontation of geologically-derived plate tectonic portraits with observed instantaneous site motions. Progress in this task followed both incremental engineering advances and the slow realization of the extent of regional deformation. Through the 1980's, it became clear that associating a

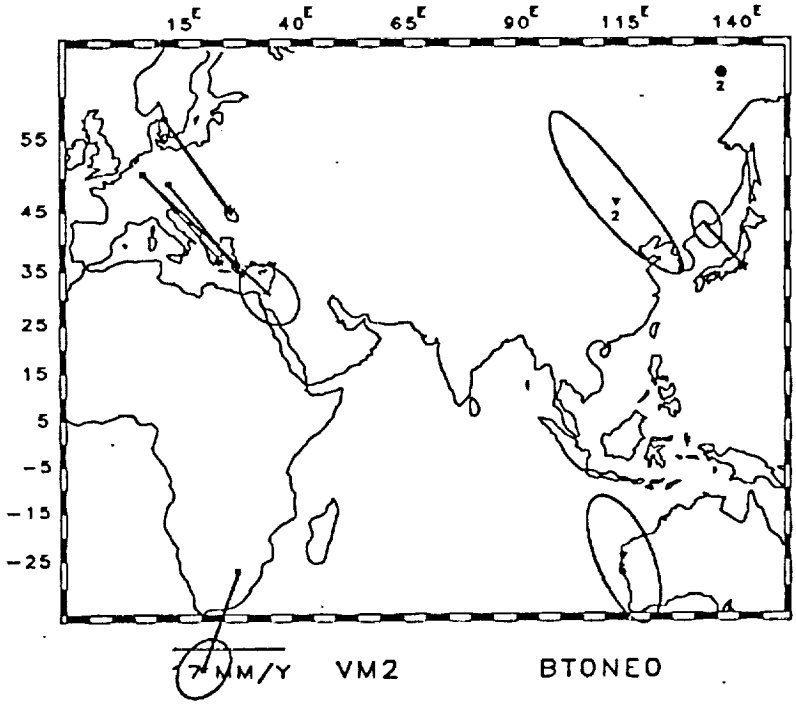

Fig. 3. VLBI vector site velocities of European, African and Japanese stations relative to North America. Circle labeled 2 in the upper right is the Europe-North American rotation pole from NUVEL-1. Inverted triangle labeled 2 is the VLBI pole enclosed in a 3 σ error ellipse. Unlike the Pacific-North America pole in Figure 2, VLBI and geologic models for European motion disagree. Measurements over the next few years should clarify this matter.

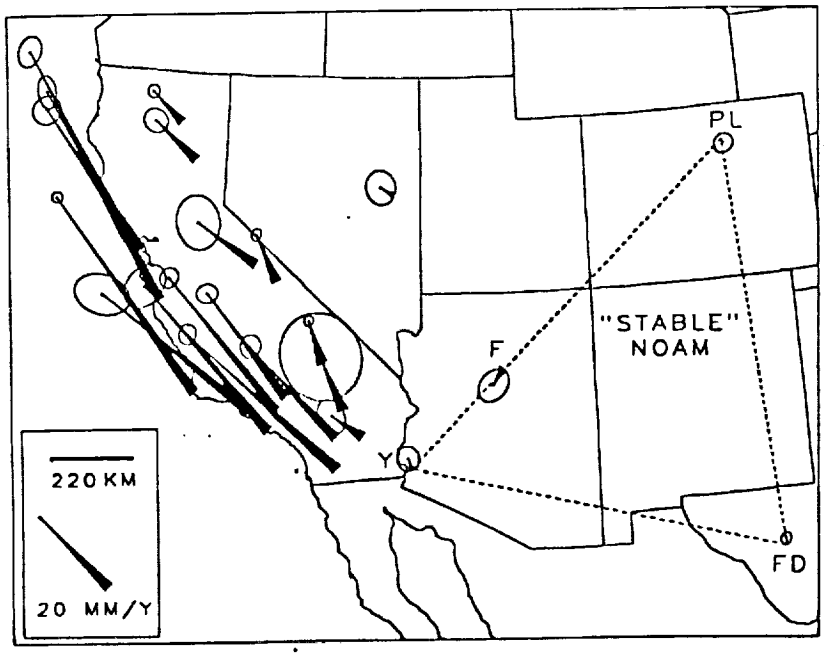

Fig. 4. Observed site velocities $\mathbf{V}_o(\mathbf{P}_i)$ for western North America and their 3σ error ellipses. Lengths of the vectors can be compared with the 20-mm/y standard vector in the box to determine site speeds. The observation frame minimizes the velocities of six interior sites on the North America plate: Ft. Davis (FD), Flagstaff (F), Platteville (PL), Yuma (Y), Westford, and Fairbanks. The stable portion of North America is reached somewhere near the Colorado Plateau.

site with a lithospheric plate was more complicated than just referencing boundaries drawn on a geologic map. For space geodetic data to contrast global tectonic motion models, it is imperative to identify stable sites, rigidly attached to the plate in question.

The Euler pole theory outlined above offers an objective and quantitative means to weed out stations which move in a manner inconsistent with the rigid plate assumption. Failure of a site to pass this test may reflect regional or local tectonics or something completely unrelated, flexure of an antenna, for instance. *Ward* [1990] showed that of the 26 United States/Pacific sites in the GLB511 solution, only 10 were consistent with rigid two plate motion. VLBI-based plate model VM2 (Figure 2), obtained by fitting vector velocities of the 10 sites in the stable interiors of the North America and Pacific plates, revealed a misfit of VLBI observations and RM2 (*Minster and Jordan*, 1978) predictions significant at the 99% confidence level. NUVEL-1 (*DeMets et al.*, 1990) reproduced the velocities of these 10 sites far better than RM2 and offered a fit to the data which is statistically indistinguishable from VM2.

In addition to North America and the Pacific, VLBI is already capable of determining plate motions for Europe, Asia and Australia (Figure 3). The observatory mode of VLBI is slated to expand through the 1990's with the North American VLBA and the Soviet QUASAR networks. This expansion should permit us to address several tectonic questions of global interest including: Asia-North America motion across the arctic, possible Asia-Europe expansion, and Asia-Australia/India compression across the Himalayas. In addition, growing VLBI ties with South America, Africa and Antarctica should provide further excitement in the coming years.

Our work in global plate motions is not strictly interpretation, but also technique development. Recently we reconsidered the use of VLBI vertical (V) and station height (Z) rates of change in equation (2) where historically, only the baseline (B) and transverse (T) rates were used to determine local north (N) and (E) velocities. Three new models were developed [BT→NEZ, BTV→NE, BTV→NEZ] and tested against the BT→NE standard. As reported at the October, 1990 CDP meeting, we found that as yet, the addition of the V and Z components fail to provide significant improvements in model consistency. As the VLBI vertical component stabilizes over the next few years, we will continue to review its status and the procedural underpinnings of our inversion.

A.3. Regional Deformation Models.

As mentioned above, one important application of space geodesy is to identify locations where rigid plate tectonics succeeds and where it fails. Judging from the behavior of western North America (Figure 4), it seems possible that motions at any continental plate boundary may deviate substantially from rigid plate theory. Where stations are sufficiently dense, as in western North America, VLBI Euler poles can quantify deformation along specific paths. For example, by including velocities of 16 additional stations in the deforming North American margin, we have resolved all four terms [$\mathbf{V}_{PN}$: Total Pacific-North America motion; $\mathbf{V}_{SA}$: San Andreas slip; $\mathbf{V}_{E,W}$: Path integrated deformation east and west of the San Andreas] in the vector equation characterizing Pacific-North America plate boundary deformation

$$\mathbf{V}_{PN} - \mathbf{V}_{SA} = \mathbf{V}_E - \mathbf{V}_W$$

for several points along the San Andreas without reference to a global plate model, geological or local geodetic measurements, or restrictions on distributed shear. In most cases, instantaneous VLBI-determined rates agree with geologically-based estimates. VLBI substantially eliminates $\mathbf{V}_W$(C), the component of the San Andreas Discrepancy west of C, although a few mm/yr of right lateral strike slip on offshore faults can not be rejected. The azimuth of San Andreas slip suggests that the transverse ranges north of Los Angeles are absorbing 8±1 mm/yr of compression perpendicular to the trend of the fault. Convergence across the transverse ranges may be slowing, judging from geological studies which infer crustal

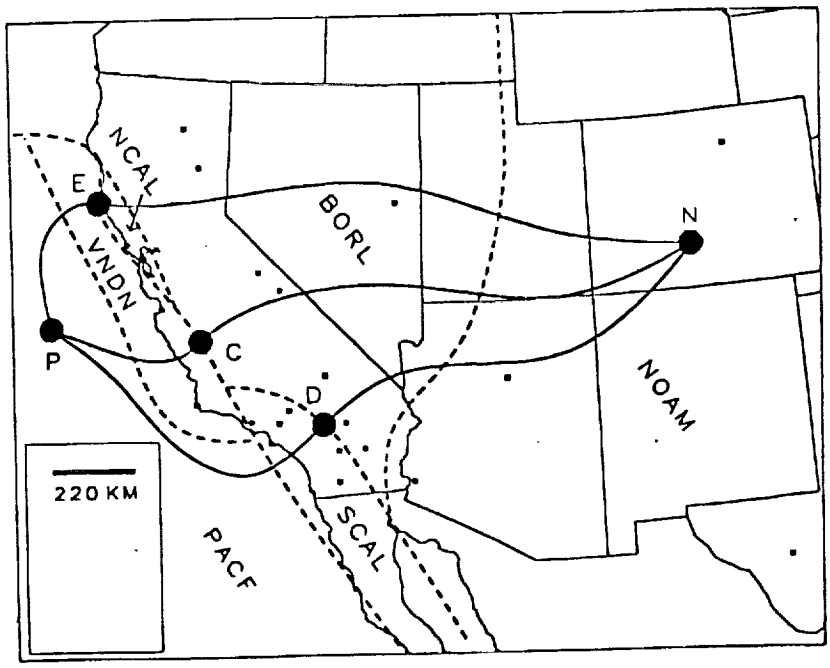

Fig. 5. Map illustrating the six plates [North America (NAM), Borderland (BLN), Northern California (NCA), Southern California (SCA), Vandenberg (VND), Pacific (PAC)] contained in the VM models. The North America plate contains the six stations: Ft. Davis, Platteville, Flagstaff, Yuma, Westford and Fairbanks. The Pacific plate contains the four sites: Vandenberg, Ft. Ord, Kwajalein and Kauai. In VM3, Vandenberg and Ft. Ord are detached onto the Vandenberg plate to test the need for offshore deformation in central California and west of the Channel Islands. Euler poles of the Borderland, Northern California and Southern California plates are used to estimate path integrated deformation along *NC*, *ND* and *NE*.

shortening rates of 17.6 to 26.5 mm/yr over the past two to three million years [*Namson and Davis*, 1988]. Along the Santa Cruz segment of the San Andreas fault which ruptured during the 1989 Loma Prieta earthquake, VM2 predicts an azimuth of Pacific-Northern California plate motion which is 16 degrees easterly from the local N46°W trend of the fault. This discrepancy is compatible with a restraining bend concept for the Santa Cruz segment and with the oblique thrust mechanism observed for the quake [*Dietz and Ellsworth*, 1990]. Even a few mm/y of fault normal motion will induce significant rates of vertical uplift and generate substantial topography in geologically short order (*Valensise and Ward*, 1991). Geodetic monitoring of evolving landforms, can, when properly modelled, discriminate modes of tectonic deformation (i.e. slip on discrete faults versus bulk shortening). In the next several years, more precise VLBI height data should play an increasing role. As one example, the Palos Verdes mobile VLBI site comes to mind. Palos Verdes is one of the fastest uplifting regions in the world, presumably due repeated slip on a buried fault. Continued measurements on this peninsula over the next several years would be useful in characterizing the unseen fault.

Along plate margins where VLBI sites are not plentiful, path integrated deformation vectors are more difficult to obtain (GPS, of course holds promise here). Nevertheless, it still is helpful to classify "normal" deformations from "abnormal" deformations. *Ward* [1988] proposed that the velocities of "normal" sites $\mathbf{P}_i$, near the boundary of Plate A and Plate B should follow

$$\mathbf{V}(\mathbf{P}_i) = \{\alpha(\mathbf{P}_i)\Omega_{AR} + [1 - \alpha(\mathbf{P}_i)]\Omega_{BR}\} \times \mathbf{P}_i;\ 0 < \alpha < 1 \qquad (3)$$

where $\Omega_{AR,BR}$ are the Euler poles of the plates and $\alpha(\mathbf{P})$ denotes the fractional association of $\mathbf{P}$ with Plate A. Equation (3) defines a polar velocity field [*Minster and Jordan*, 1984]

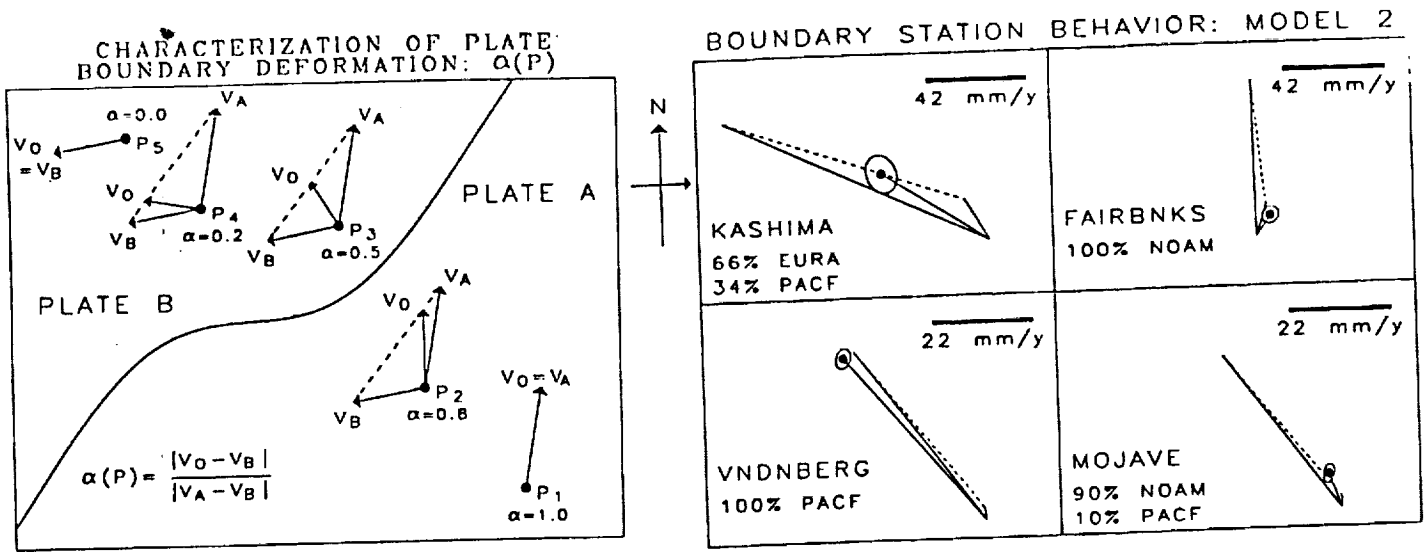

Fig. 6. Left. Cartoon illustrating the behavior of a "normal" plate boundary. For normal sites, the VLBI-determined velocity $\mathbf{V}_o$, should follow equation (3) and fall on the dotted line connecting $\mathbf{V}_A$ and $\mathbf{V}_B$, the predicted rigid plate velocities. Note how boundary deformation can obscure measures of relative plate rates. To gauge true relative motion, velocities of sites $\mathbf{P}_1$ and $\mathbf{P}_5$ in the stable interior must be compared. Including sites $\mathbf{P}_2$, $\mathbf{P}_3$, or $\mathbf{P}_4$ in rigid plate motion estimates would induce significant bias. *Right.* Application of equation (3) to selected plate boundary sites. All of these sites are behaving "normally".

and simplifies the interpretation of vector deformations to that of characterizing a scalar function. *Ward* [1988] found that velocities (3) fit 88% of the VLBI measurements in the western United States when $\alpha(\mathbf{P}_i)$ was restricted to a two parameter linear transition, and 95% of the measurements when $\alpha(\mathbf{P}_i)$ was allowed to be free at each station.

Figure 6 (*left*) cartoons a "normal" plate boundary at which α varies monotonically across the margin. Points $\mathbf{P}_1$ and $\mathbf{P}_5$, located in the stable interior of the plates, travel at velocities $\mathbf{V}_a$ and $\mathbf{V}_b$ predicted by rigid plate theory. Closer to the frontier, rigid plate theory fails as the lithosphere deforms. Near the margin, $\mathbf{V}_o$, the instantaneous site velocity, is not likely to be either $\mathbf{V}_a$ or $\mathbf{V}_b$, but a mixture described by equation (3). Depending on the elastic-plastic composition of the borderlands, strain developing at plate boundaries partitions into recoverable and permanent components. If recoverable elastic elements are present, then $\alpha(\mathbf{P}_i)$ is really $\alpha(\mathbf{P}_i, t)$, a function of time through the earthquake cycle. Averaged over many cycles, the velocities of borderland sites may or may not be equal to that observed at any given epoch. Distinctions between geological and instantaneous strain accumulation at plate boundaries however, can not affect estimates of Euler poles derived from stations in stable plate interiors as these sites have no knowledge of distant earthquake cycles.

Over the next several years we will continue to classify the kinematics of plate margins through path integrated deformation vectors where possible (North America, Mediterranean, Alaska) or through $\alpha(\mathbf{P}_i)$ (*right*, Figure 6). Kinematic classification is the first step toward a dynamic analysis.

B. VLBI and Earthquake Prediction.

Observations of large scale strain accumulation are indispensable inputs for any master

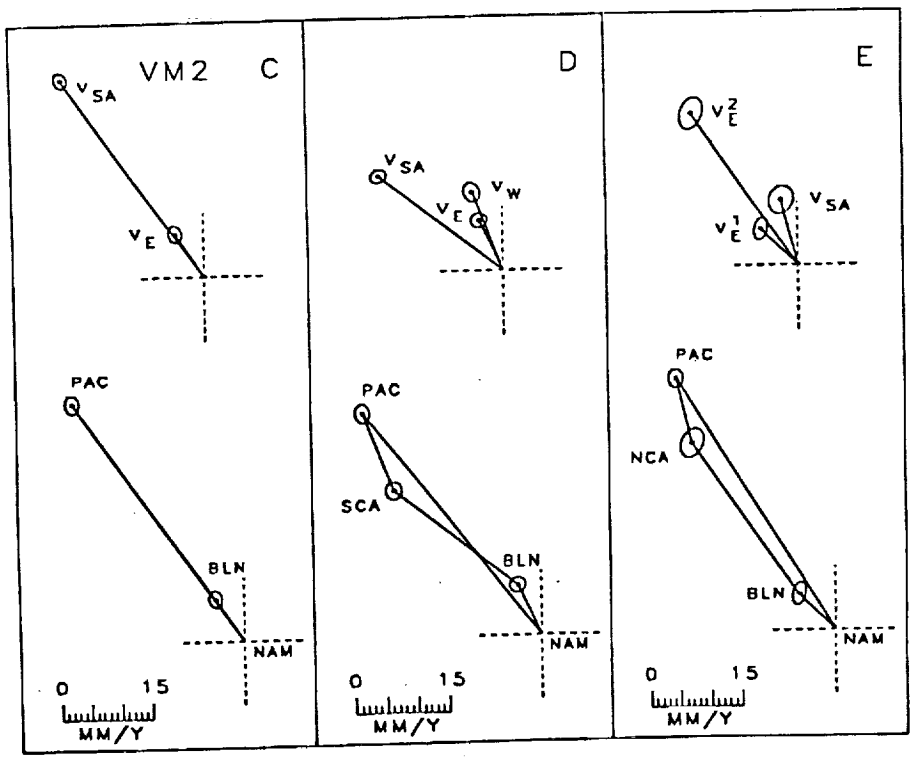

Fig. 7. Individual (*Top*) and summed (*Bottom*) plate motion vectors V_{PN}, V_{SA}, V_E and V_W for VM2 projected on the tangent plane at points C, D and E of Figure 5. Error ellipses are 3σ. VLBI-determined slip rates at points C, D and E on the San Andreas are 38.6±1.3 mm/y (N36°±2°W), 25.0±1.1 mm/y (N52°±3°W), and 10.6±2.1 mm/y (N14°±11°W) respectively. Segments BLN-NAM represent accumulated deformation across the Basin and Range. Segments PAC-BLN, SCA-BLN and PAC-NCA represent the San Andreas slip rates at C, D and E.

model of earthquake prediction. For instance, one would think that the single most important number controlling earthquake hazard in the western United States is the rate of relative motion between the Pacific and North America Plates. *Minster and Jordan's* [1978] RM2 value of 5.5 cm/yr, for instance, has been built into innumerable models of earthquake recurrence. Until recently, rates of plate motion in the historical past could be obtained only by indirect methods. Today, space-geodetic techniques not only allow relative plate motions to be measured directly, but also reveal where strain is distributed. In California, VLBI has provided the first truly instantaneous estimates of slip rates along various sections of the San Andreas (Figure 7) and the first determinations of Euler poles for lithospheric sub-plates of the region. In southern California, we find a much slower rate of San Andreas slip [25.0 mm/yr (N24°W)] than along the central coast. Most of the decrease [13.3 mm/yr (N21°W)] is accommodated in the southern California borderland west of the San Andreas to the Channel Islands. Approximately 9 mm/yr of motion taken up by the Basin and Range will be transferred to the San Andreas and manifested in steadily increasing slip rates south of the Salton Sea. VLBI supports local geodetic evidence (*Prescott et. al.*, 1981) for a pronounced decrease in San Andreas slip in Northern California. About 15-20 mm/yr of Pacific-North America motion is siphoned off to faults east and north of the San Francisco Bay.

VLBI has further suggested several aspects of the tectonic control of earthquake faults. When taken together, the six VLBI sites on the Southern California plate (SCA) dictate a

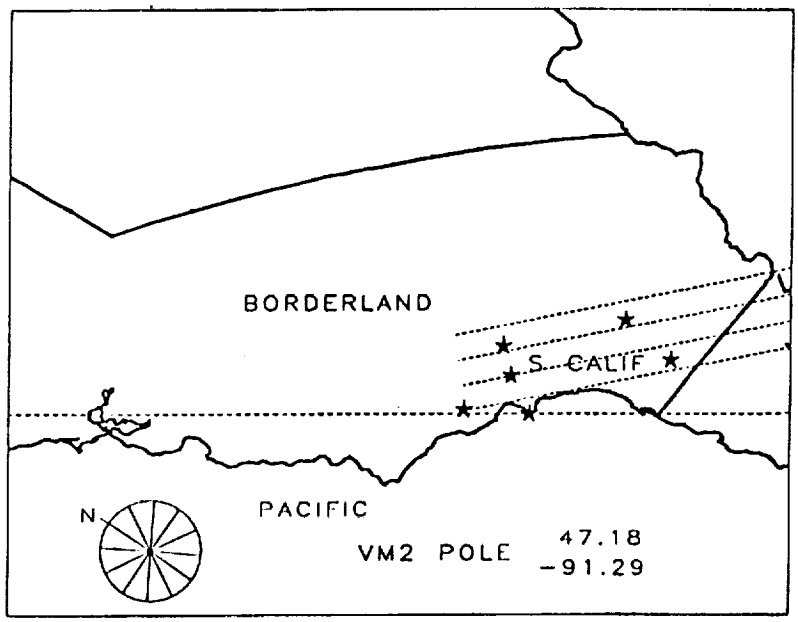

Fig. 8. Oblique Mercator projection of California about the VLBI-determined Pacific-Borderland pole of rotation (47.18°N, 91.29° W). Because the Borderland has roughly 9 mm/y of N25°W motion relative to stable North America, a projection about the PAC-BOR pole is more relevant than the more conventional projection about the PAC-NAM pole. The six VLBI sites in southern California (*stars*), when placed on a single rigid plate (SCA), dictate a motion relative to the Borderland which is 11° more westerly than PAC-BOR motions. Long and short dashed lines are small circles about the PAC-BOR and SCA-BOR poles respectively.

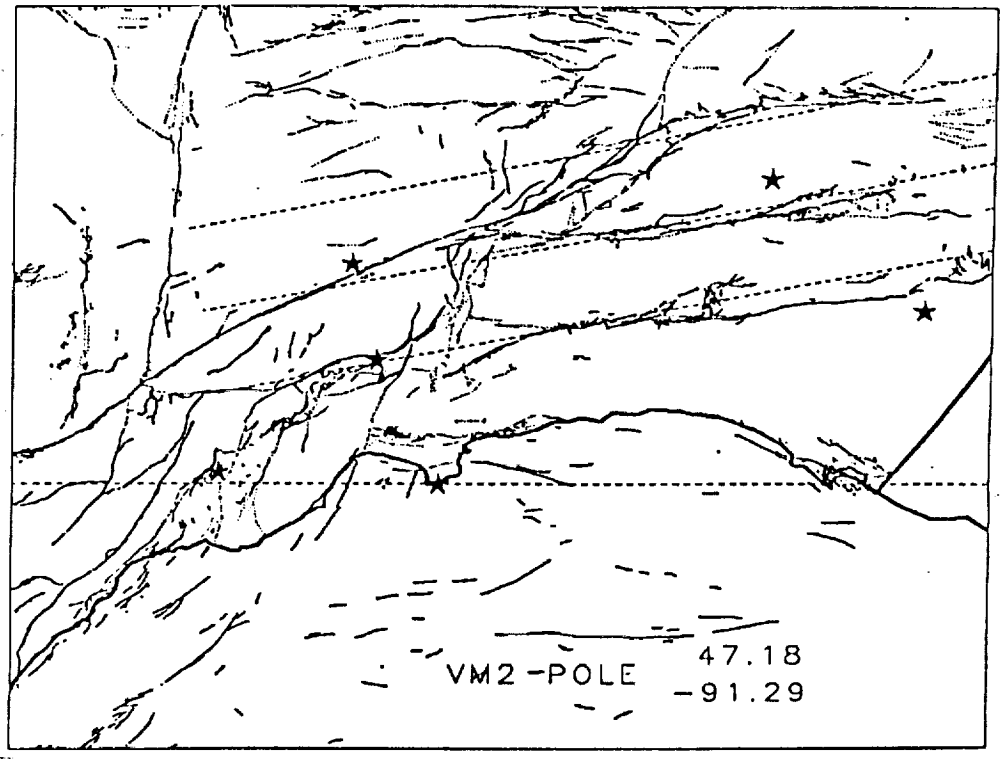

Fig. 9. Blow up of southern California showing Pleistocene faults. Small circles about the SCA-BOR pole (inclined dashed lines) are suggestive of the trends of the Elsinore and San Jacinto faults. Loosening of the rigid plate assumption and further localization of relative motions among the various faults are priorities for future research.

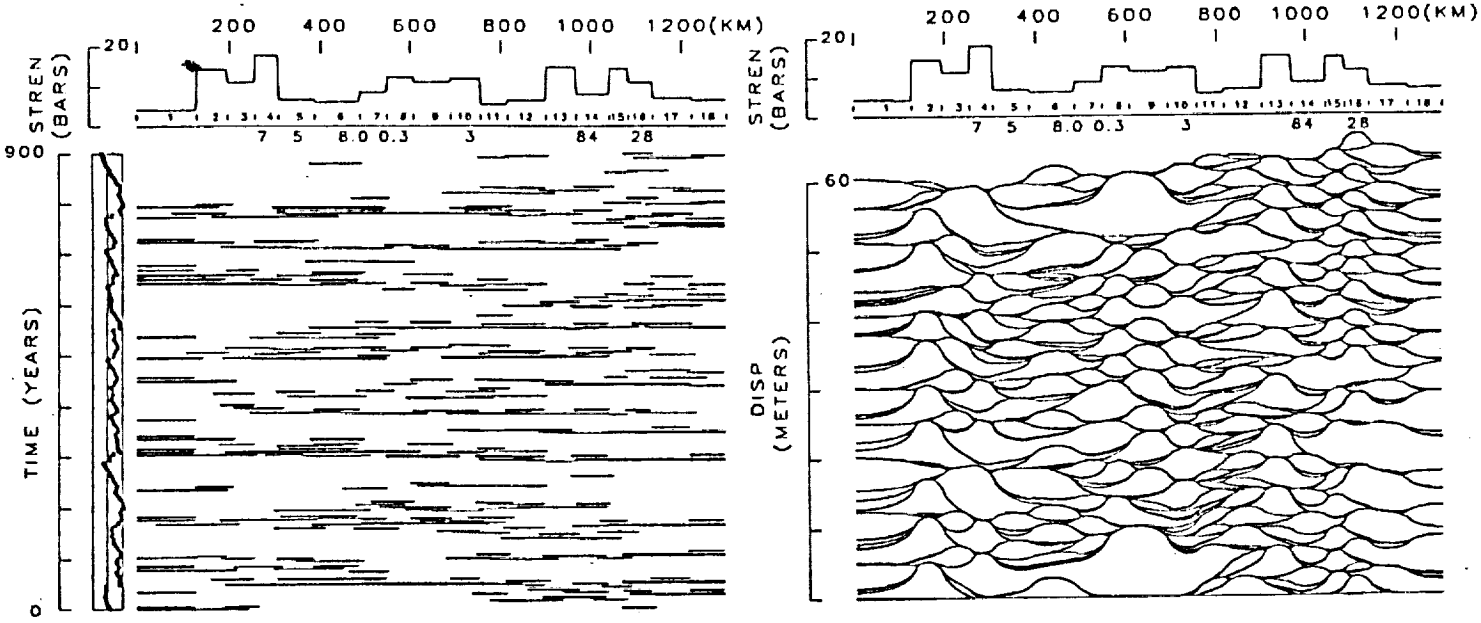

Fig. 10. Left. Synthetic space-time seismicity ($M \geq 7$) plot for a hypothetical plate boundary covering a 900 year time span. The sawtooth curve along the top shows the distribution of lengths and strengths for the 18 segments comprising this realization of the boundary. Over about 200 years, the complex interaction of fault segments and the non-linear failure conditions conspire to transform an apparently deterministic model to a chaotic one, in that small changes in initial conditions ultimately lead to very different patterns of earthquakes. *Right.* Plot showing the accumulation of tectonic displacement along strike. Each pillow represents the slip resulting from one of the discrete events to the left. Averaged over time, all of the segments must maintain a plate tectonic rate of 7 cm/yr. Note how some segments (#15, for instance) display a greater fraction of characteristic earthquakes (*Schwartz and Coppersmith*, 1984) than others (eg. #4).

sense of motion relative to the North America Borderland (BOR) which is 11° more westerly than Pacific-Borderland motion (Figure 8). Most likely in an effort to minimize obliquity (angular mismatch of relative fault displacement and fault strike), the Elsinore and San Jacinto faults (Figure 9) have aligned themselves along small circles about the SCA-BOR pole. On the San Andreas, obliquity migrates from fault-normal tension near the Salton Sea to fault-normal compression east of Los Angeles. The details of how the obliquity of SCA-BOR and PAC-SCA motions are accommodated remain a major concern for earthquake hazard evaluation (eg. blind thrusts). It is a concern in which VLBI will play an important role for the foreseeable future.

The pattern of earthquakes along even a simple plate boundary can be complex, and there is growing evidence that the seismic moment release may be only a fraction of the total slip budget. Lately, we have made strides in modeling synthetic seismicity and fault interaction (Figure 10). These models, based on static dislocation theory (*Bonafede et. al.*, 1985; *Dragoni*, 1990), assist in localizing geodetic experiments and provide guides for the magnitude of the signals to be expected. The slip patches in Figure 10 could occur seismically or aseismically. VLBI has previously detected coseismic signals associated the the 1989 Loma Prieta earthquake (*Clark et al.*, 1990) and the 1988 Alaskan sound event, and should have no trouble detecting any $M \geq 7$ slip event, even if it occurs aseismically. Combining synthetic seismicity models with observed motions of the Alaskan sites, for example, should clarify the partitioning of strain transfer among the region's great strike slip and thrust faults systems (Figure 11). Our speculation is that the high velocity of Yakataga is largely permanent, the

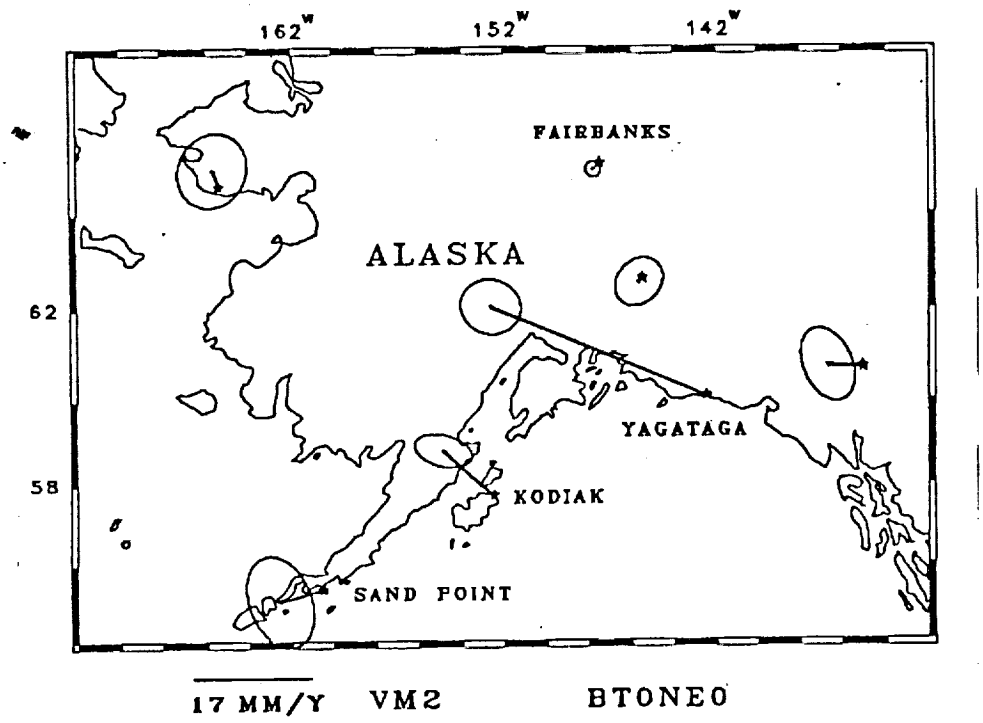

Fig. 11. Map of VLBI-determined site velocities in Alaska relative to North America. We suspect that the high velocity of the Yakataga site reflects permanent strain taken up on interior faults.

motion being taken up inboard.

The VLBI network is continuously expanding and improving. The data employed in *Ward* [1990] is already two years old. In that interval, there have been several reoccupations including: Vernal Utah, Kwajalein and the Alaskan sites. Recovering the motion of Vernal is key toward identifying the eastward limit of Basin and Range expansion. Refinement of the Kwajalein velocity will, oddly enough (through reduction of the uncertainty in Pacific plate stability), help put to rest the question of the slip rate on the San Gregorio- Hosgri fault. (Both marine terrace data and VLBI suggest to us that this is probably a fossil feature.) With continued NASA funding we will update velocity estimates with the newest measurements and attempt to further isolate the deformation field through the introduction of multiple or non-rigid tectonic plates.

C. IMPORTANCE OF MOBILE VLBI IN THE 1990's.

The successes we now enjoy in interpreting tectonics from VLBI data have been ten years in the making. Much of the progress, certainly in the area of regional deformation, has to be credited to the mobile VLBI program. At the March 1991 working group meeting in Pasadena, NASA headquarters expressed sentiments that mobile VLBI has outlived its usefulness and indicated that it will not play any role in the CDP follow-on program. I consider the elimination of mobile VLBI to be a sad turn of events. The costs saved in terminating mobile VLBI have to be weighted against the likely scientific return. In geodetic monitoring of tectonics, continuity is critical. The long history and consistency of VLBI observations at many sites through the western United States and Alaska will not be duplicated by replacement technologies for many years, if ever. Mobile VLBI measurements touch upon almost every aspect of the work proposed here. If these lines of research are viewed as a valuable component of the Dynamics of the Solid Earth NRA, then I would argue strongly that mobile VLBI campaigns must continue at some level through the 1990s.

References

Bonafede, M., M. Dragoni and E. Bochi, Quasi-static crack models and the frictional stress threshold criterion for slip arrest, *Geophys. J. R. Astr. Soc., 83*, 615 - 635, 1985.

Clark, T. A. et al., Geodetic measurement of deformations in the Loma Prieta, California earthquake with very long baseline interferometry, *Geophs. Res. Lett., 17*, 1215-1218, 1990.

Demets, C., R. G. Gordon, S. Stein, and D. F. Argus, Current Plate Motions, *Geophys. J., 101*, 425 - 478, 1990.

Dietz, L. and W. Ellsworth, The October 17, 1989 Loma Prieta, California, earthquake and its aftershocks: Geometry of the sequence from high-resolution locations, *Geophys. Res. Lett., 17*, 1417 - 1420, 1990.

Dragoni, M., A model of interseismic fault slip in the presence of asperities, *Geophys. J. R. Astr. Soc., 101*, 147 - 156, 1990.

Gordon, D., C. M. Ma, T. A. Clark, and J. W. Ryan, Site velocities from the Crustal Dynamics Project VLBI geodynamics database, (abstract), *EOS*, 1988.

Minster, J. B., and T. H. Jordan, Present-day plate motions, *J. Geophys. Res., 83*, 5331 - 5334, 1978.

Namson, J. and T. Davis, Structural transect of the western Transverse Ranges, California: Implications for lithospheric kinematics and seismic risk evaluation, *Geology, 16*, 675 - 679, 1988.

Prescott, W. H., Lisowski, M. & Savage, J. C., Geodetic measurement of crustal deformation on the San Andreas, Hayward and Calaveras faults near San Francisco, California, *J. Geophys. Res., 86*, 10853 - 10869 , 1981.

Schwartz, D. P., and K. J. Coppersmith, Fault behavior and characteristic earthquake: examples from the Wasatch and San Andreas fault zones, *J. Geophys. Res., 89*, 5681 - 5698, 1984.

Ward, S. N., North America-Pacific Plate Boundary, and Elastic-Plastic Megashear, Evidence from VLBI, *Jour. Geophys. Res., 93*, 7716 - 7728, 1988.

Ward, S. N., North America-Pacific Plate Motions: New Results from Very Long Baseline Interferometry, *Jour. Geophs. Res., 95*, 21,965 - 21,982, 1990.

Ward, S.N., Synthetic Seismicity Models of the Middle American Trench, *in preparation*, 1991.

Valensise, G. and S.N. Ward, Long-Term Uplift of the Santa Cruz Coastline in Response to Repeated Earthquakes along the San Andreas Fault, *Bull. Seism. Soc. Am.*, in press, 1991.

Recent Publications Supported by this Project

Barrientos, S.E. and S.N. Ward, 1990. The 1960 Chile Earthquake: Inversion for Slip Distribution from Surface Deformation, *Geophys. J. Int., 103*, 589-598.

McNally, K. and S.N. Ward, 1990. The Loma Prieta Earthquake of October 17, 1989: Introduction to the Special Issue, *Geophys. Res. Lett., 17*, 1177.

Ward, S.N., 1990. North America-Pacific Plate Motions: New Results from Very Long Baseline Interferometry, *J. Geophys. Res., 93*, 21,965-21,981.

Valensise, G. and S.N. Ward, 1991. Long-Term Uplift of the Santa Cruz Coastline in Response to Repeated Earthquakes along the San Andreas Fault, *Bull. Seism. Soc. Am.*, in press.

Ward, S. N., 1991. Synthetic Seismicity Models for the Middle American Trench, *J. Geophys. Res.*, submitted.